Development, modelling and control of a micro/nano positioning 2DoF stick-slip device.

Micky Rakotondrabe, Yassine Haddab, Philippe Lutz

Development, modelling and control of a micro/nano positioning 2DoF stick-slip device

Micky Rakotondrabe, *member, IEEE*, Yassine Haddab and Philippe Lutz, *member, IEEE*

***Abstract*— The works presented in this article are motivated by the high performances required in micromanipulation/microassembly tasks. For that, this paper presents the developement, the modelling and the control of a 2 degrees of freedom (in linear and angular motion) micropositioning device. Based on the stick-slip motion principle, the device is characterized by unlimited strokes and submicrometric resolutions. First, experiments were carried out to characterize the performances of the micropositioning device in resolution and in speed. After that, a state-space model was developed for the sub-step functioning. Such functioning is interesting for a highly accurate task like nanopositioning. The model is validated experimentally. Finally, a controller was designed and applied to the micropositioning device. The results show good robustness margins and a response time of the closed-loop system.**

***Index Terms*— Micropositioning device, stick-slip, linear and angular motion, state-space modelling, postioning control.**

I. Introduction

NOwadays, the need of miniaturized systems with complex functions is in constant growth. Microfabrication technologies are not always suitable to produce such systems, particularly hybrid systems (i.e. combining several functions: mechanical, electrical, thermal, optical, etc.). For them, microassembly is better adapted. To manipulate and to assemble microproducts, especially MEMS (MicroElectroMechanical Systems), the use of conventional assembly systems leads to major difficulties because of the scale effects (adhesion forces [1], lack of precision ...). In order to take into account these scale effects, a complete study of the actuators, the sensors and the production methods must be made. Also, production systems should have dimensions which are adapted to those of the products. These systems are called microfactories and consist of microssembly and micromanipulation stations.

As the microcomponents of the microproducts (MEMS for example) generally have dimensions between $10\mu m$ and $2mm$, it is very interesting to use stations that are able to handle such a range of dimensions. However, a very high positioning accuracy is required in microassembly. It is generally micrometric or submicrometric. So the positioning devices should have submicrometric resolution. Finally, to pick, transport and place a component from one location to another, in order to complete the assembly, the devices must have a high stroke motion.

FEMTO-ST Institute, UMR CNRS 6174 - UFC / ENSMM / UTBM
Automatic Control and Micro-Mechatronic Systems depart., AS2M
24, rue Alain Savary
25000 Besançon - France
corresponding authour: mrakoto@femto-st.fr
Paper type: regular paper.
Technical area: Robotics.

For these reasons, a microgripper device with a large gap, high stroke and high resolution is of interest. Two possibilities may be used.

- First, one can use a high stroke positioning device coupled with a microgripper (Fig. 1-a), examples in [2] [3]. In order to cover the range of the components sizes, different microgrippers with different gaps are required. The advantage of this solution is that the resolution of the large stroke device does not necessarily have to be very high if the resolution of the microgrippers is. However, a system able to exchange the different microgrippers is required [4].
- The second solution is the use of two or more independant devices with high stroke which collaborate together in order to pick, transport and place the components (Fig. 1-b). In this case, the gap of the microgripper is naturally unlimited. The references [5] [6] are two examples of this concept. While microgrippers are not necessarily useful, the concept necessitates positioning devices with a high stroke and a high resolution.

As part of our microfactory project, the latter concept was chosen. We describe in this paper the development of a micropositioning device dedicated to a microfactory station. Another important aspect in microassemby is the need of

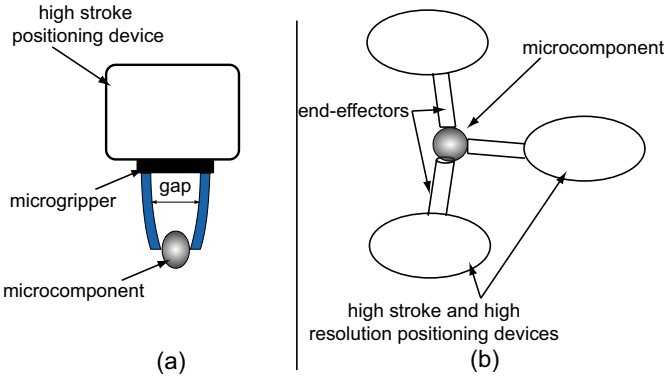

Fig. 1. a: a high stroke positioning device coupled with a microgripper. b: several high stroke and high resolution positioning devices in collaboration.

higher dexterity. As the shapes of the MEMS become more and more complex, positioning devices with a higher number of degrees of freedom (DoF) are needed. The microrobots presented in [7] [8] [9] are good examples. Each of them has 3DoF (x-y linear motions and z angular motion).

On the other hand, the automation of microassembly stations is interesting because the productivity rate can be increased.

However, the higher the number of DoF is, the higher the complexity of the automation of positioning devices in collaboration is. A compromise has to be found. We propose the kinematic structure of a microassembly and micromanipulation station as shown in Fig. 2. The station consists of two devices each having one 2DoF (linear and angular). One axis supports both the devices in order to increase the ease of their collaboration. This paper reports the development of one 2-DoF micropositioning device based on the stick-slip principle.

When fine positioning is needed in a task, the use of the displacement within a step (sub-step), i.e. within a stick-phase, is prefered. During the fine positioning mode, the disturbances may influence the success of the task. These disturbances may be the variation of the load, the environment (temperature and pressure) and so on. In addition, good performances are often necessary for the tasks. They are the response time, the statical error and the bandpass. To ensure the disturbances rejection and the robustness in performances, a closed loop control of the positioning device is recommended. Two control modes are also possible for that: the coarse mode control and the fine mode control. For the former, a first approach is the use of a basic algorithm (*if error > one step, then apply a step*) [10]. Another approach is the control of the amplitude of the periodic input signal [11]. Concerning the fine mode, [12] uses a 2^{nd} order model and an adaptive sliding mode control to perform while [13] obtains a 4^{th} order model and computes a polynomial digital controller to perform the precise positioning. These controllers are dedicated to only one mode. It is also possible to compute one controller which takes into account both the fine and coarse functioning modes [14] [10]. Notwithstanding, using dedicated controllers remain the best way to obtain good performances because the specifications can be efficiently taken into account during the synthesis. Motivated by the need of high accuracy in micromanipulation/microassembly tasks, we present in this paper the modelling and control of the sub-step (fine) positioning of the developped micropositioning device.

The paper is organized as follows. First, the development of the micropositiong device is presented. Then, its performances are detailed. After that, a state-space model is developed for the sub-step functioning. The identification of parameters and the validation of the whole model are presented. Finally, the synthesis and the implementation of a PI controller is given. The phase and gain margins of the closed-loop system are high and can ensure the stability and the performances facing the uncertainties on the numerical values of the different parameters of the models.

II. General description of the micropositioning device

A. Target System

First, we present the wanted characteristics of the microsystem:

- the device has two degrees of freedom: linear and angular motions,
- the desired resolution is greater than $1\mu m$,
- in each motion, a very high stroke has to be possible: more than $5cm$ in the linear motion and $360°$ in the angular one,
- finally, the device has to have adequate dimensions: a maximum volume of $2cm \times 2cm \times 2cm$.

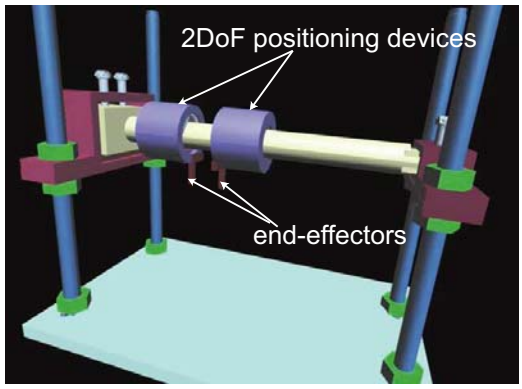

Fig. 2. Principle of the micrompanipulation station.

B. Presentation of the used microactuators

There are different principles to obtain the high stroke and the high resolution characteristics of a micropositioning device. They can be classified into principles with embedded microactuators and principles with non-embedded microactuators. It is obvious that those with embedded actuators may offer a theoretically infinite stroke. Among these principles, the stick-slip one is very interesting for two reasons: the compactness of the used microactuators and the simplicity of the control signal (just the use of a sawtooth signal). Stick-slip actuators are generally based on piezoelectric materials. Two modes of motion can be obtained with a micropositioner using stick-slip actuators: the stepping mode and the sub-step mode. The stepping mode consists in applying a sawtooth voltage to the micropositioner and letting it move step by step, in high range and with a high velocity on the workspace (Fig. 3-a, b and c). The resolution in this mode is limited to one step. When the difference between the reference position and the present postion becomes smaller than a step, the legs (piezoelectric actuators) are bent slowly until the final position is reached (Fig. 3-d). This is the sub-step mode and the obtained resolution can be very high.

In [15], a stick-slip microactuator called *push-pull* microactuator is proposed. It offers the possibility to perform several DoF from only one bulk material. Due to its characteristics, we use this microactuator in 2-DoF configuration (Fig. 4-a and b) to move our micropositioning device. The microactuator is based on a piezoelectric layer. There are four electrodes on the upper face and one electrode on the electrical ground in the lower face. They constitute the active parts of the microactuator. A sapphire disk-shaped foot is glued on the latter. When a positive electrical potential is applied to two electrodes while the opposite potential is applied to the other two, one half of the active part contracts while the second one expands. Thus, the foot performs a displacement δ and a rotation (Fig. 4-c). Now, let us place the microactuator on

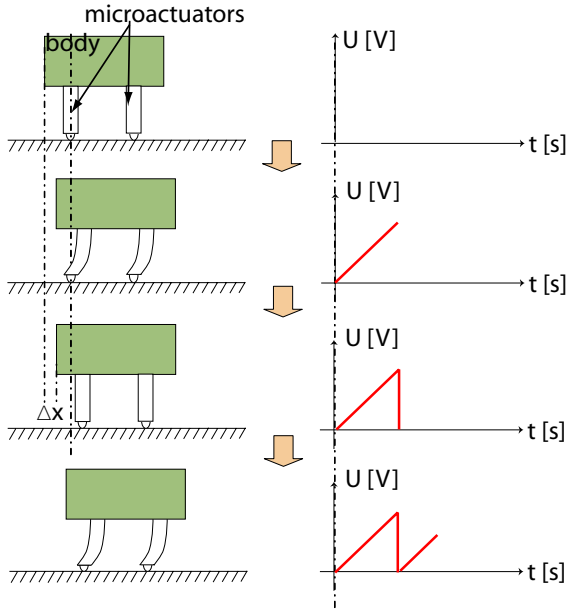

Fig. 3. Stick-slip principle. a, b and c : stepping mode. d : sub-step mode.

a base. If the preload $\overrightarrow{N}$ is high enough, there is no rotation of the foot and the displacement of the microactuator only depends on δ (Fig. 4-d). The stick-slip motion is obtained when applying a saw-tooth voltages to the electrodes. While the foot is in contact with the base, the nonactive surface of the upper face will be glued with the body of the micropositioning device (hatched area in the Fig. 4-a).

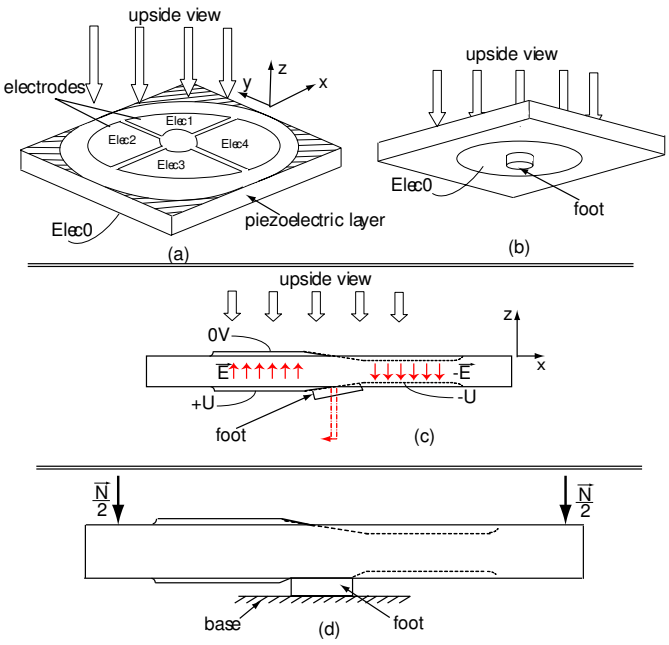

Fig. 4. a (upside view) and b (underside view): the push-pull microactuator with 2-DoF configuration [15]. c: displacement and rotation of the foot. d: displacement of the microactuator on a base.

C. Integration of the microactuators on the 2-DoF device

This part presents the integration of the above microactuator inside the 2-DoF device in order to move it. A cylindrical tube is used to support the device. This is the base on which the microactuator will be placed. The upper face of the microactuator is embedded in the device body while the foot is in contact with the tube. We especially use a glass-tube because the contact between glass and sapphire materials has optimal friction characteristics:

- during the stick-phase, a sufficient adherence is performed so the loss of displacement is minimized,
- during the slip phase, the friction is relatively low so the issued overheating is minimized. Such overheating may destroy the microactuators elements (sapphire, etc.).

To maintain the axial guidance of the device on the tube, at least two contact points are necessary. However, to maintain the radial guidance, at least three contact points spread out over $360°$ are necessary. So we use six contact points to maintain the device on the tube. All the contact points are represented by microactuators in order to obtain a maximal total torque when they are activated simultaneously. The two "axial-guidance" microactuators form a pair of microactuators and glued together on an alumina support in order to facilitate their integration (Fig. 5-a and b). A system for the adjustment of the radial force is introduced for each pair of microactuators (Fig. 5-c and d). It is based on two tilted plates (lower and upper) and a screw. Through the plates, the adjustment of the screw will move the microactuator back-and-forth and then increases or decreases the radial force. It is used to preload (nominal radial force) the microactuators. However, the glass-tube presents a high cylindricity default and the micropositioning device may work imperfectly. To solve that, the third tilted plates system is replaced by an adaptable spring-system (Fig. 5-e). The lateral spring maintains the microactuator pinned against the body while the radial spring compensates the default of the tube. The adaptable springs are built by folding and shearing a thin metallic plate ($thickness = 0.05mm$) (Fig. 5-f).

Besides the dimensions, the weight is the main criteria of the design because of the limited torque that the microactuators can deliver. This is why the optimized shape of the body minimizing the weight is a triangle (Fig. 5-b). The body is made of alumina material. We call the whole device the 'TRING'-module (Triangular RING module). Due to the complexity of the shape and the smallness of the dimensions, the body of the TRING-module was fabricated with Electric-Discharge technology. The Fig. 6 shows the TRING-module on its tube.

III. Characterisation of the TRING-module

A. Step characteristics

Here, we evaluate the amplitude of a step of the microsystem in linear and in angular motions.

1) Linear motion: in linear motion, we perform the measurements with an interferometer with a $1.24nm$ resolution. The Fig. 7-a shows a linear displacement of the microsystem with a sawtooth voltage with $150V$ of amplitude and $500Hz$ of frequency. We remark that the step is quasi constant during

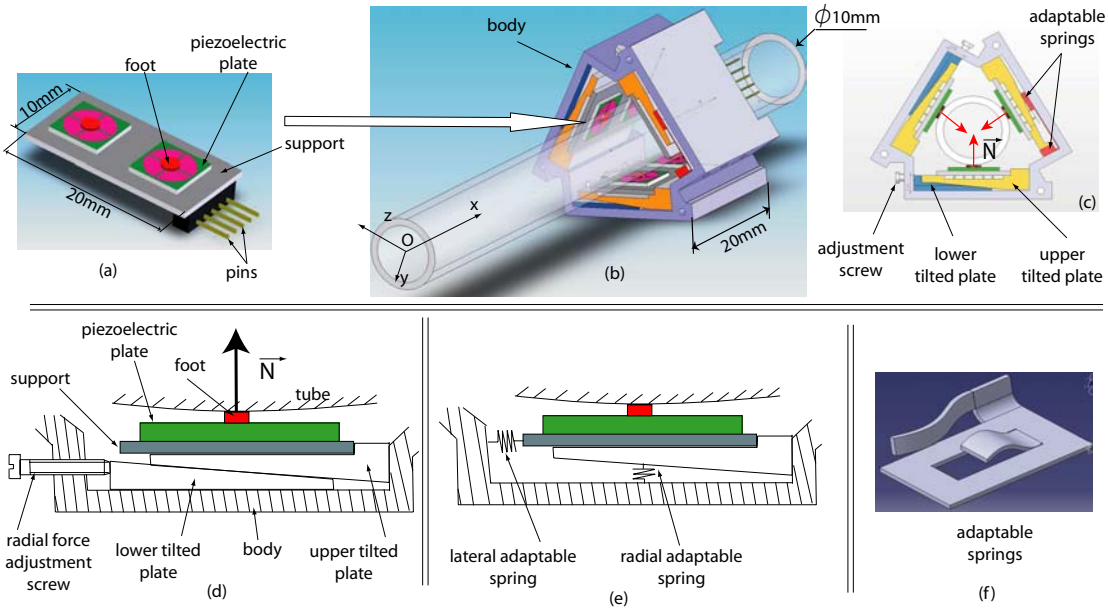

Fig. 5. a: a pair of microactuators is glued onto a support. b and c: three pairs of microactuators are spread out inside the device. d: a tilted-plate system is used to adjust the nominal radial force. e and f: an adaptable spring-system is used to compensate the cylindricity defect of the tube.

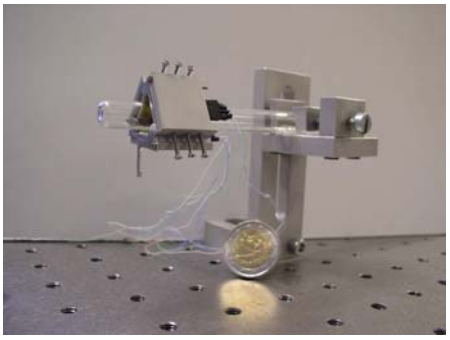

Fig. 6. A photograph of the TRING-module on the glass-tube.

the displacement. Fig. 7-b is a zoom of one step. We can notice the oscillations during the stick-phase caused by the step signal of the previous slip-phase. They are due to the dynamic of the microactuators and the mass of the TRING-module. The maximal step, obtained with $150V$, is about $200nm$. Decreasing the amplitude will decrease the value of the step and will then increase the resolution of the micropositioning device. As example, with $U = 75V$ the step is approximatively $70nm$. However, whatever the amplitude is, the step efficiency is constant. The step efficiency is defined as the ratio between the gained step and the amplitude of the applied voltage [16] :

$$\eta_{step} = \frac{step}{\Delta amp} \approx 0.7 \qquad (1)$$

2) Angular motion: as we do not have an accurate appropriate sensor to measure the angular motion, we use the linear sensor and apply the measurement principle shown in Fig. 8. Let θ represent the angle of displacement of the microsystem, dl be the tangential displacement and $R_{meas} \approx 2cm$ be a

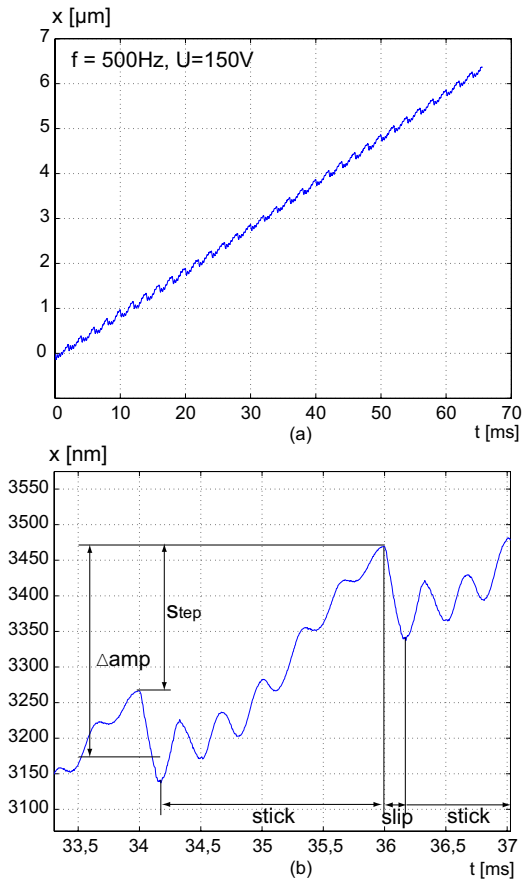

Fig. 7. Linear displacement measurement of the TRING-module using an interferometer. a: a series of stick-slip obtained with $U = 150V$ and $f = 500Hz$. b: vibrations inside a step obtained with $U = 150V$ and $f = 60Hz$.

radius. Around the characterisation point, we have:

$$\theta \approx \frac{dl}{R_{meas}} \quad (2)$$

The experiments give a step of $0.0025°$ with $U = 150V$,

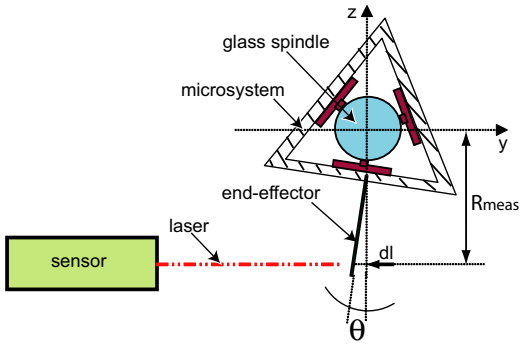

Fig. 8. The principle of measurement during angular motion.

$0.0015°$ with $U = 100V$ and $0.001°$ with $U = 75V$. Of course, the radius R_{meas} is not exactly known and the used value is approximative. As its uncertainty is bounded by $\pm 2cm$, the uncertainty on θ is bonded by $\pm 10\%$.

B. High stroke characteristics

Here, the capability of the TRING-module in terms of speed is analyzed. The analysis is done with different values of frequency and amplitude. To measure the displacement, we use an optical sensor with $500nm$ of resolution and $\pm 4cm$ of range for the linear motion while an accelerometer with $1°$ of accuracy and $\pm 90°$ of range for the angular one is used.

1) Linear motion: Fig. 9 summarizes the speed performances of the TRING-module in linear motion. The spectrum (Fig. 9-a) indicates the linearity of speed versus frequency (for a given voltage amplitude). Above $10kHz$, saturation and disturbances appear. They are due to the bandpass limit and to the eigen frequencies of the microactuators and of the entire structure. We can also remark the linearity of speed versus amplitude (for a given frequency) (Fig. 9-b). The applied maximal amplitude is $150V$ in order to avoid destruction or depolarization of the piezo microactuators. Below $35V$, the device cannot have a high stroke motion because there is not enough torque to provide the sliding. It only moves back and forth following the microactuators. The maximal speed is about $1.8mm/s$ and it is obtained when the frequency is $10kHz$ and the amplitude $150V$. A test gives the maximal force that the TRING-module can deliver. For that, we use a spring with a known stiffness and which is pushed by the device. When the speed of the latter becomes null, the maximal force is obtained: $150mN$. This is good enough for the manipulation of small parts.

2) Angular motion: To measure angular displacement, we use a capacitive based sensor from FREESCALE: $weight < 2g$, dimensions $2mm \times 6mm \times 6mm$. Due to its smallness, it is easily inserted into the TRING-module. It has a measurement stroke of $\pm 90°$ and the accuracy depends on the electronic filter and amplifier. As we only take an interest in the high

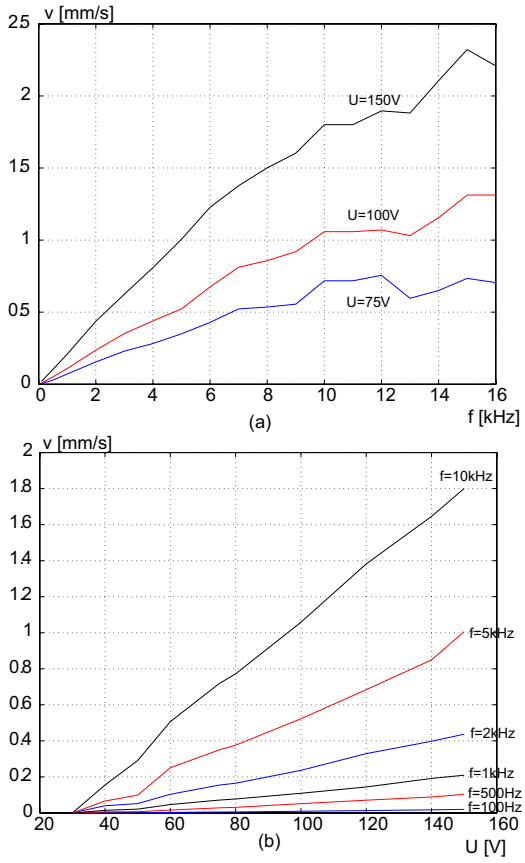

Fig. 9. Speed performances in linear motion.

stroke motion, the used accuracy is $\pm 0.5°$. Fig. 10 shows speed performances. The same remarks made about the linear motion can be derived: frequency linearity up to $10kHz$ and minimal voltage for displacement about $35V$. Maximal speed is about $20°/s$, i.e. nearly $18s$ for one complete rotation.

IV. Sub-step modelling of the TRING-module

Here, we develop a state-space model of the TRING-module working in sub-step. There are two reasons why we want to model it: firstly, to ease the synthesis of a controller, secondly, to help the design of the microactuator from given performances.

A. Main assumptions

The study of the microsystem is reduced to the study of one microactuator with a mass on it. The radial force $\overrightarrow{N}$ applied on each microactuator will be called normal force. The weight of the microsystem is weak in comparison with the result of the normal forces. The manipulation force (load) is not introduced here since it is considered as a disturbance. The adhesion forces between the foot and the spindle are insignificant in relation to the normal force. The base (tube) and the foot are assumed to be rigid and no vibration appears on the tube because we only work in stick-phase. During this phase, the foot and the tube are stuck and then there is no shock causing any vibration.

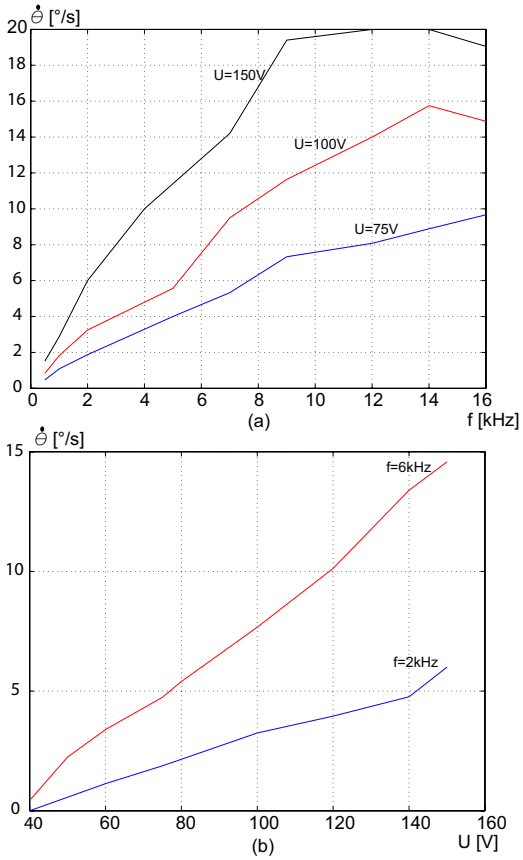

Fig. 10. Speed spectrum in angular motion.

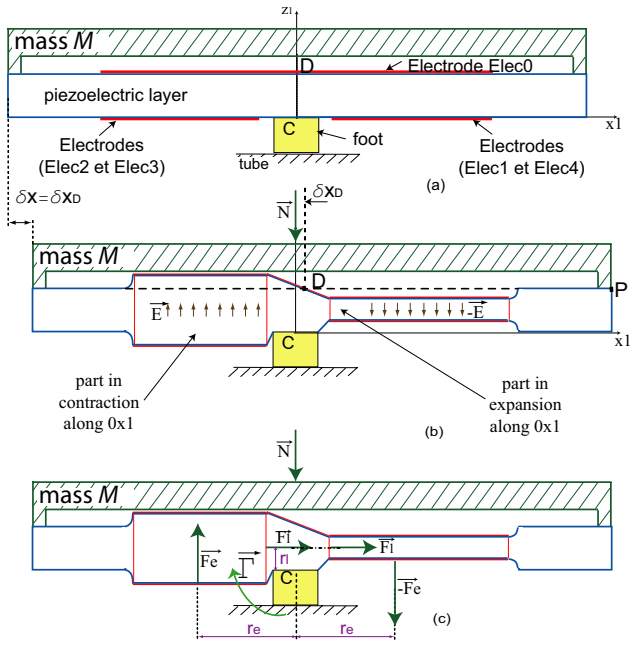

Fig. 11. a: the mass M is glued on the non-active area of the microactuator. b and c: strain of the microactuator.

B. Working equations

Two parts are considered here: the determination of the piezoelectric working equation and the determination of the friction working equation. The former gives the internal states of the piezoelectric microactuator while the latter gives the internal state of the friction. We will apply the fundamental principle of the dynamics to combine them and to obtain the model of the whole device.

1) Piezoelectric working equation: Fig. 11-a shows one microactuator placed on a base. The mass M is composed of: the mass of one piezoelectric actuator, one tilted-plate system and a sixth of the body's mass. Cx_1z_1 represents the local referential in the symetric plane of the piezoelectric layer. Point C represents the center of the contact surface between the foot and the layer. Point D is the center of the upper surface (Fig. 11-b). A displacement δx_D of D generates a displacement δx of the TRING-module body with the same amplitude and direction. The aim of this subsection is to find the displacement of point D relative to point C. When we apply two symetrical voltages ($+U$ and $-U$) to the electrodes, the piezoelectric layer warps (Fig. 11-b). We assume that the radial force $\vec{N}$ is sufficient to maintain all the lower surface of the foot pinned against the base. Let us isolate the piezoelectric layer. We can summarize the following important parameters (Fig. 11-c):

- the resultant force $\overrightarrow{F}$ and the resultant torque $\overrightarrow{\Gamma}$ relative to point C,
- the scalar fields δx, δy and δz which respectively indicate the displacement fields along Cx_1, Cy_1 and Cz_1 inside the piezoelectric layer. Let δx_D be the value of δx, δy_D the value of δy and δz_D the value of δz at point D. We assume that δy_D and δz_D are null. Thus, we only focus our study on the evaluation of δx_D.

The resultant force $\overrightarrow{F}$ consists of:

- the normal force $\overrightarrow{N}$. $\overrightarrow{N}$ is assumed to be reduced to point D. When $\delta x_D \neq 0$, we consider that $\overrightarrow{N}$ still stays coaxial with the principal axis of the foot because δx_D is small in relation to the surface.
- the normal reaction $-\overrightarrow{N}$ applied on point C by the foot to the piezo layer,
- two equivalent forces $\overrightarrow{F_e}$ and $-\overrightarrow{F_e}$ are applied to the half active parts of the piezo layer. They are parallel to the electric field. Each of the forces is applied at an equivalent distance r_e from the principal axis. We assume that r_e is constant whatever the strain δx_D is, the latter being negligible compared with the former,
- a lateral force $\overrightarrow{F_l}$ is applied to each part of the layer. This force is perpendicular to the electric field and is assumed to be at an equivalent distance r_l from the upper surface of the foot. We can consider that r_l is constant whatever the deformation of the piezo layer is because δz_D is null.

The equivalent forces F_e, $-F_e$ and F_l are due to the fact that the foot is constrained in rotation. Foremost, let us study the equation of the two active parts. For that, Sx indicates the contraction (or expansion) of one active part along the Cx_1 axis. In the case of a parallelepipedal layer characterized by a length L, a width w and a thickness e (Fig. 12-a), the transversal strain equation of the piezo layer can be derived

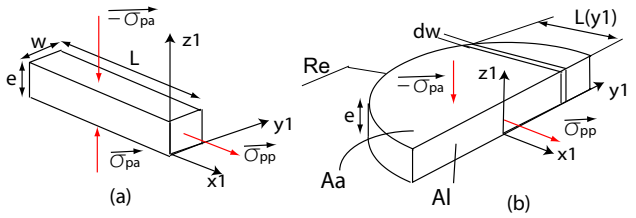

Fig. 12. a: a parallelepiped piezo layer. b: a hemicylindrical piezo layer.

using [17]:

$$Sx = d_{31} \cdot \frac{L}{e} \cdot U + s_{13} \cdot L \cdot \sigma_{pa} + s_{11} \cdot L \cdot \sigma_{pp} \quad (3)$$

where:

- $d_{31} < 0$, $s_{13} > 0$ and $s_{11} > 0$ are respectively the transversal piezoelectric constant, the transversal elastic constant and the axial elastic constant,
- σ_{pa} and σ_{pp} represent the mechanical stresses respectively parallel and perpendicular to the electrical field, the electrical field being parallel with z_1 axis,
- e is the thickness at rest (without strain) and $E \approx \frac{U}{e}$.

Notwithstanding, the shape of one active part of the microactuator is not parallelepipedal but hemicylindrical with a radius R_e (Fig. 12-b). It can be considered as a sum of parallelepipeds with a constant width dw and a y_1 dependent length written $L(y_1)$. However, to facilitate the equation of the axial strain Sx, we introduce a shape coefficient c_{oeff} inside the (equ 3):

$$Sx = c_{oeff}. \left(d_{31}. \frac{R_e}{e}.U + s_{13}.R_e.\sigma_{pa} + s_{11}.R_e.\sigma_{pp} \right) \quad (4)$$

The previous equation is related to only one active half part. In spite of this, the displacement δx_D can be constructed with the strain of the two half active parts. As the two parts are symmetric, we can use the (equ 4) in introducing a correction coefficient c_{orr}. Considering $q = c_{orrD}.c_{oeff}$, we obtain:

$$Sx = q. \left(d_{31}. \frac{R_e}{e}.U + s_{13}.R_e.\sigma_{pa} + s_{11}.R_e.\sigma_{pp} \right) \quad (5)$$

Let us now evaluate the stresses σ_{pa} and σ_{pp}. Let A_a be the area on which the equivalent force $\overrightarrow{F_e}$ is applied and A_l the area on which the lateral force $\overrightarrow{F_l}$ is applied (Fig. 12-b). We have:

$$\sigma_{pa} = \frac{F_e}{A_a} \quad (6)$$

$$\sigma_{pp} = \frac{F_l}{A_l} \quad (7)$$

On the other hand, if we isolate the foot, we have:

$$F_{mp} = -2.F_l \quad (8)$$

$$\Gamma_{mp} = F_{mp}.h_c \quad (9)$$

where F_{mp} and $\Gamma_{mp} = -\Gamma$ are respectively the force and the torque applied to the foot by the piezo layer. The height of the foot is represented by h_c. It is reminded that two vertical forces defined by $\overrightarrow{N}$ and $\overrightarrow{-N}$ are also acting on the foot. As their sum equals zero, they will not be considered. Moreover, using a previous assumption stating that $\overrightarrow{N}$ stays co-axial with the foot, the latter force does not influence the torque Γ_{mp}.

Using (equ 5)-(equ 9), and noting that $\delta x = \delta x_D$, we infer:

$$\delta x = q. \frac{\mathrm{R}_e}{e}. [d_{31}.U - e.k.F_{mp}] \quad (10)$$

with:

$$k = \frac{h_c.s_{13}}{2.r_e.A_a} + \frac{s_{11}}{2.A_l} - \frac{r_l.s_{13}}{2.r_e.A_a} \quad (11)$$

The (equ 10) is a static model. To complete this, we assume that the piezo layer has a second order dynamic behaviour. A higher order would complicate the model, a lower order (first order) is not sufficient if the system has a resonance frequency. If a and b respectively represent the inertial and the viscous parameters of the piezo layer, the working equation is:

$$\frac{d\dot{\delta x}}{dt} = \frac{q.\mathrm{R}_e}{a.e}. [d_{31}.U - e.k.F_{mp}] - \frac{b}{a}.\dot{\delta x} - \frac{1}{a}.\delta x \quad (12)$$

2) Equations of the friction: In the previous part, we determined the displacement of mass M in relation to point C (the foot). In this part, we determine the displacement x_C of point C in relation to the base and thus to the reference $\Re_0$. In fact, during the stick-phase, the pre-displacement due to the deflexion of the asperities may have an amplitude with an order of magnitude equivalent to δ_x. In addition, if the state of the friction can be expressed, it will be easy to control the force friction in order to maintain the device working in stick-phase. According to the applications there are several models of friction [18] but the one which allows the modelling of the stick-phase is the *single-state elastoplastic model* [19]. The application of this model to our case (stick-phase and no lubricant) gives:

$$f_f = -N \cdot \rho_0 \cdot x_C \quad (13)$$

where f_f indicates the deflexion resistance of the medium asperity, ρ_0 represents the Coulomb parameter.

C. State equations

Here, we write the state-equations of the micropositioning device in linear and in angular motions. The voltage U is considered as the input variable.

First, let us study the case of linear motion. Fig. 13-a represents the system when a voltage U is applied. As we only consider the stick-phase, we can assume that the reference $\Re_0$ has an origin at the contact between the base and the tip of the medium asperity. In this figure, $\overrightarrow{R}$ is the reaction of the base and is composed of the normal force $-\overrightarrow{N}$ and the tangential force $\overrightarrow{T}$. This latter is the friction. The real system (Fig. 13-a) can be approximated by Fig. 13-b where m_p is the mass of the foot and m incorporates the mass M and the mass of the piezo layer. We assume that the point D coincides with the center of the mass m. We also assume that there are no rotation components either for m_p or for m. If we isolate the mass m, from the precedent remarks and the accelerations law, we have:

$$\ddot{x} = \ddot{x}_C + \ddot{\delta x} \quad (14)$$

where x indicates the displacement of the mass m in relation to the reference $\Re_0$. The external forces applied to m are

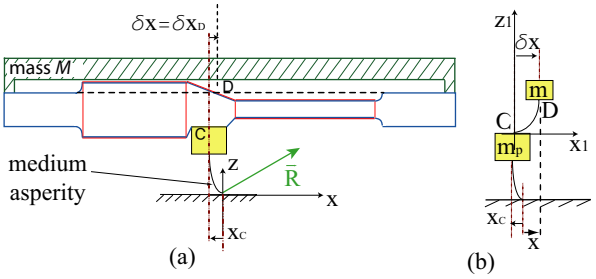

Fig. 13. Scheme of the stick-phase. The dimension of asperity is blown up in order to see its deflexion.

composed of: 1) the force $F_{pm} = -F_{mp}$ applied by the foot, 2) and the manipulation force applied by the manipulated component. This latter is assumed to be negligible. If not, it may be considered as an external disturbance. Applying the dynamics law to m and using the (equ 14), we can write:

$$\ddot{x}_C + \ddot{\delta}x = \frac{-F_{mp}}{m} \tag{15}$$

On the other hand, isolating the foot lead us to the following dynamics expression:

$$\ddot{x}_C = \frac{1}{m_p}.\left(F_{mp} - N.\rho_0.x_{as}\right) \tag{16}$$

From the piezo working equation (equ 12), the dynamics of m in (equ 15) and the dynamics of the foot (equ 16), we have the following expressions:

$$\frac{d\dot{\delta}x}{dt} = \frac{1}{m_{equ}}.\left(q.\frac{\mathrm{R}_e}{e}.d_{31}.U - k_1.x_C - b.\dot{\delta}x - \delta x\right) \tag{17}$$

$$\frac{d\dot{x}_C}{dt} = \frac{k_m}{m_{equ}}.\left(-q.\frac{\mathrm{R}_e}{e}.d_{31}.U + k_2.x_C + b.\dot{\delta}x + \delta x\right) \tag{18}$$

with:

$$\left\{\begin{array}{c} k_m = \frac{m}{(m_p+m)} \\ m_{equ} = a - m_p.k_m.q.\mathrm{R}_e.k \\ k_1 = k_m.q.\mathrm{R}_e.k.N.\rho_0 \\ k_2 = k_1 - \frac{N.\rho_0.m_{equ}}{m} \end{array}\right. \tag{19}$$

1) State equation of the linear mode: Using the equations (equ 17) and (equ 18), we infer the state-space model of the TRING-module:

$$\frac{d}{dt}\begin{pmatrix}\delta x\\ \dot{\delta}x\\ x_C\\ \dot{x}_C\end{pmatrix} = \begin{pmatrix}0 & 1 & 0 & 0\\ -\frac{1}{m_{equ}} & -\frac{b}{m_{equ}} & -\frac{k_1}{m_{equ}} & 0\\ 0 & 0 & 0 & 1\\ \frac{k_m}{m_{equ}} & \frac{b.k_m}{m_{equ}} & \frac{k_2.k_m}{m_{equ}} & 0\end{pmatrix}.\begin{pmatrix}\delta x\\ \dot{\delta}x\\ x_C\\ \dot{x}_C\end{pmatrix} + \begin{pmatrix}0\\ \frac{q.\mathrm{R}_e.d_{31}}{e.m_{equ}}\\ 0\\ -\frac{k_m.q.\mathrm{R}_e.d_{31}}{e.m_{equ}}\end{pmatrix}.U \tag{20}$$

2) State equation of the angular mode: Let us notice δs and s_C respectively the internal state of the piezo layer and the internal state of the medium asperity during the angular mode. As the displacement δs and s_C are very small in relation to the radius of the tube, we can consider that there are no rotation components in the angular mode. The state equation of the two modes are then similar. We have:

$$\frac{d}{dt}\begin{pmatrix}\delta s\\ \dot{\delta}s\\ s_C\\ \dot{s}_C\end{pmatrix} = \begin{pmatrix}0 & 1 & 0 & 0\\ -\frac{1}{m_{equ}} & -\frac{b}{m_{equ}} & -\frac{k_1}{m_{equ}} & 0\\ 0 & 0 & 0 & 1\\ \frac{k_m}{m_{equ}} & \frac{b.k_m}{m_{equ}} & \frac{k_2.k_m}{m_{equ}} & 0\end{pmatrix}.\begin{pmatrix}\delta s\\ \dot{\delta}s\\ s_C\\ \dot{s}_C\end{pmatrix} + \begin{pmatrix}0\\ \frac{q.\mathrm{R}_e.d_{31}}{e.m_{equ}}\\ 0\\ -\frac{k_m.q.\mathrm{R}_e.d_{31}}{e.m_{equ}}\end{pmatrix}.U \tag{21}$$

D. Output equations

The output vector has two variables during the stick-phase: the total friction T and the displacement x (for the linear motion) or the angle θ (for the angular motion). Indeed, while the displacement is the main interest of the model, in some applications it is important to estimate or control the friction. For example, if one wants to always ensure the sub-step functioning mode, the friction T is controlled to be lower than a limit friction such as the stick-mode is always guaranteed. If we isolate the foot, we can easily infer that the friction $T = F_{pm}$. To determine this, we use the (equ 16).

1) Output equation of the linear mode: We have:

$$\begin{pmatrix}T\\ x\end{pmatrix} = \begin{pmatrix}-\frac{m.(1-k_m)}{m_{equ}} & -\frac{m.b.(1-k_m)}{m_{equ}} & -\frac{m.(k_1-k_2.k_m)}{m_{equ}} & 0\\ 1 & 0 & 1 & 0\end{pmatrix}.\begin{pmatrix}\delta x\\ \dot{\delta}x\\ x_C\\ \dot{x}_C\end{pmatrix} + \begin{pmatrix}\frac{m.q.\mathrm{R}_e.d_{31}.(1-k_m)}{e.m_{equ}}\\ 0\end{pmatrix}.U \tag{22}$$

2) Output equation of the angular mode: Fig. 14 represents the simplified scheme of the motion of D in the angular mode. We can approximate $s_D = R_D.\theta$, where s_D is the approximated displacement of D ($s_D = \delta s + s_C$) and R_D the distance between the point D and the spindle axis at rest.

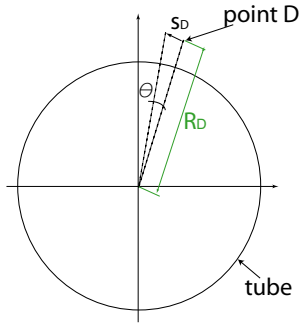

Fig. 14. The angle θ is one of the output variables in the angular mode of the stick-phase.

Thus, the output equation in the angular mode is:

$$\begin{pmatrix} T \\ \theta \end{pmatrix} = \begin{pmatrix} -\frac{m\cdot(1-k_m)}{m_{equ}} & -\frac{m\cdot b\cdot(1-k_m)}{m_{equ}} & -\frac{m\cdot(k_1-k_2\cdot k_m)}{m_{equ}} & 0 \\ \frac{1}{R_D} & 0 & \frac{1}{R_D} & 0 \end{pmatrix} \cdot \begin{pmatrix} \delta s \\ \dot{\delta} s \\ s_C \\ \dot{s}_C \end{pmatrix} + \begin{pmatrix} \frac{m\cdot q\cdot \mathrm{R}_e\cdot d_{31}\cdot(1-k_m)}{e\cdot m_{equ}} \\ 0 \end{pmatrix} .U \tag{23}$$

V. Parameters identification and validation of the sub-step model

In this section, we identify the unknown parameters of the above sub-step modelling. They are the coefficient q, the inertial and the viscous parameters a and b. After identification, we will validate the whole model both for the statical and the dynamical modes. The rest of the parameters are presented in the Table I.

Due to the lack of an accurate angular sensor, we only process the linear motion mode. This does not allow a loss of generality because the angular motion model has the same parameters as the linear motion model except the radius of the tube. We use an interferometer of $1.24nm$ resolution for the experiments.

Using the state-space equation (20) and the output equation (22), we derive the transfer function relating the sub-step displacement x and the voltage U:

$$G_{xU} = \frac{x(s)}{U(s)} = \frac{q.\,\mathrm{Re}\,.d_{31}}{e}\cdot\frac{\left(b_2^{num}.s^2+1\right)}{\left(a_4^{den}.s^4+a_3^{den}.s^3+a_2^{den}.s^2+a_1^{den}.s+1\right)} \tag{24}$$

with:

$$\begin{cases} b_2^{num} = \dfrac{m_{equ}}{k_m.\,(k_1-k_2)} \\ a_4^{den} = \dfrac{m_{equ}^2}{k_m.\,(k_1-k_2)} \\ a_3^{den} = \dfrac{b.m_{equ}}{k_m.\,(k_1-k_2)} \\ a_2^{den} = \dfrac{m_{equ}.\,(1-k_2.k_m)}{k_m.\,(k_1-k_2)} \\ a_1^{den} = b \end{cases} \tag{25}$$

In addition to the parameters identification, the transfer function described in (24) will be used to synthesize a controller in the next section.

TABLE I

Physical and geometrical parameters.

Dimensions:	
e	$0.5mm$
h_c	$0.5mm$
r_e	$0.5mm$
r_l	$0.25mm$
R_e	$3mm$
gap	$0,2mm$
A_l	$5mm^2$
A_a	$0.367mm^2$
Other parameters:	
d_{31}	$-210\times10^{-12}m/V$
s_{11}	$19\times10^{-12}m^2/N$
s_{13}	$15\times10^{-12}m^2/N$
m	$1g$
m_e	$1.562mg$
ρ_0	$1.583\times10^9m^{-1}$
N	$1N$

A. Identification of the parameter q

The steady-state form of the transfer function (24) is:

$$q = \frac{x.e}{d_{31}.\,\mathrm{R}_e\,.U} \tag{26}$$

On the other hand, when the steady-state is reached, the deflection of the medium asperity becomes null. Thus, To determine q, a statical analysis with a piezoelectric actuator can be performed. Considering the smallness of the piezo layer, it is impossible to isolate it and to carry out experiments. A statical analysis with a FEM method (with ANSYS) was then performed. We apply a voltage of $150V$. The corresponding displacement is $x = 142nm$. Thus, we have $q = 0.7515$.

B. Validation of the steady-state model

To validate the structure of the steady-state equation (26) and the determined value of q, we compare the corresponding simulation with an experimental result for different values of U. Fig. 15 shows that the curves align well.

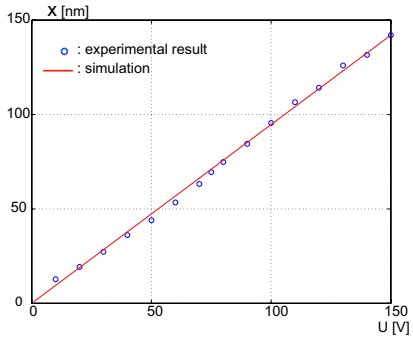

Fig. 15. Validation of the static regime and the identified parameter q.

C. Identification of the parameters a and b

Considering the smallness of the piezo layer, it is impossible to isolate them and determine the parameters a and b. Thus, we perform a harmonic analysis of one microactuator with a FEM method (with ANSYS). We obtain $a = 9.77 \times 10^{-10}[s^2]$ and b = $200 \times 10^{-6}[s]$.

D. Validation of the whole model

To validate the whole model (24) with the different identified parameters, we use a harmonic experimental analysis of the TRING-module. The chosen amplitude of the sine voltage is $75V$ instead of $150V$. Indeed, with a high amplitude, the minimum frequency from which the drift starts is low. In the example of Fig. 16, a frequency of $2250Hz$ already derives a drift when the amplitude is $150V$ while a frequency of $5000Hz$ does not when it is $75V$. The higher the amplitude is, the higher the acceleration is and consequently the higher the risk of sliding (drift) is. When the TRING-module slides, the sub-step model is no longer valid. Fig. 17 presents the magnitude of the simulation of the equation (24) and the experimental result. It shows that the structure of the model and the identified parameters are befitting.

VI. Control of the sub-step functioning

The aim of the sub-step control is to improve the performances of the TRING-module during a high accurate task and to reject the disturbances (manipulation force, adhesion forces, environment). Indeed, when positioning a microcomponent, the manipulation force can disturb the positioning task and modify its accuracy. In addition, the numerical values of the parameters (physical and geometrical) are uncertain. Thus, we want to introduce high stability margins in the closed-loop system.

The sub-step functioning necessitates that the derivate of the voltage $\frac{dU}{dt}$ should be inferior to a maximum slope $\dot{U}_{\max}$. A rate-limiter is then introduced in the closed-loop scheme in order to limit the slope of U (Fig. 18-a).

A proportional controller was first applied. Due to the non-negligible statical error, an integrator was afterwards added. For the closed-loop system, we want to have a phase-margin of $60°$. To calculate the corresponding proportional gain K_p and integrator gain $K_i = \frac{1}{T_i}$ (T_i is the integrator time parameter),

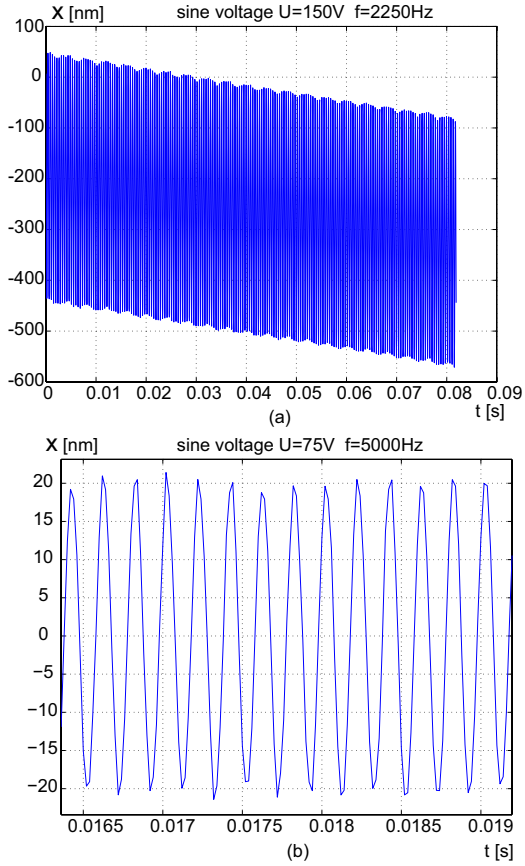

Fig. 16. The outbreak of a drift of the TRING-module happens at low frequency when the amplitude is high.

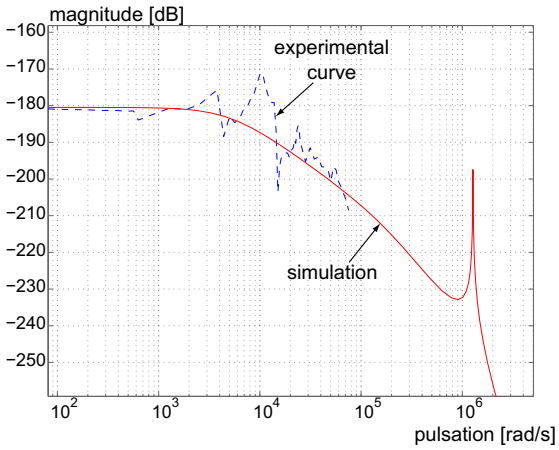

Fig. 17. Validation of the complete model.

we trace the Black-Nichols diagram of the open loop system G_{xU} (Fig. 19). Let $K_{PI} = K_p \cdot \left(1 + K_i \cdot \frac{1}{s}\right)$ be the transfer function of the controller. The $60°$ of margin phase is obtained if the new open loop transfer function $K_{PI} \cdot G_{xU}$ has a Black-Nichols diagram which cuts the $0dB$ horizontal axis at $240°$. The goal is then to compute a corrector K_{PI} which moves the diagram of Fig. 19 up to the wanted diagram. For that, we choose a point of the initial diagram and move it up to the point $(0dB, 240°)$. As the integrator provides a delay, the

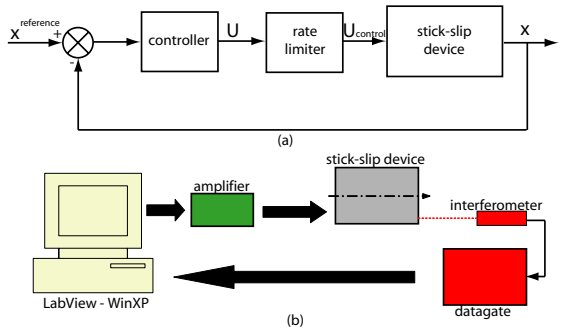

Fig. 18. a: structure of the closed-loop system. b: setup structure.

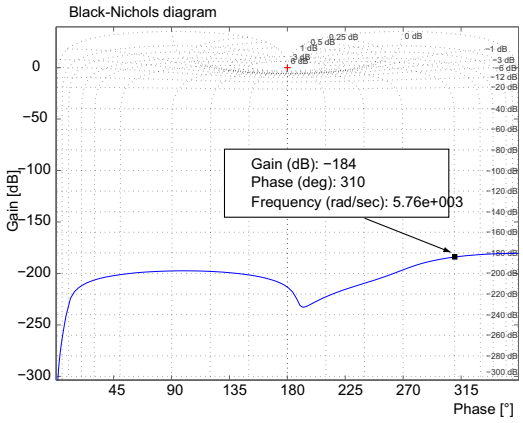

Fig. 19. Black-Nichols diagram of G_{xU}.

chosen point should have a phase which is more than $240°$. We take $(-184dB, 310°)$ (Fig. 19). This point is obtained with a frequency of $\omega_0 = 2.89 \times 10^3 rad/s$. After that, two operations are applied:

- addition of a gain of $184dB$. The corresponding ratio is $g_K = 1122018454$,
- application of the phase delay due to the integrator: $\varphi_i = 310° - 240° = 70°$.

From this data, we have:

$$T_i = \frac{1}{\omega_0 . \tan(\varphi_i)} = 125.94 \times 10^{-6} \quad (27)$$

$$\gamma = \frac{Ti.\omega_0}{\sqrt{1 + (Ti.\omega_0)^2}} = 0.3420 \quad (28)$$

Where γ is the gain at high frequency. We directly infer:

$$K_p = \gamma . g_K = 383749529 \quad (29)$$

$$K_i = \frac{1}{T_i} = 7940 \quad (30)$$

The controller was implemented following the principle-scheme in Fig. 18. The reference displacement is a step input signal $x^{reference} = 100nm$. Because the voltage generated by the controller is rate-limited, the settling-time relative to the step input is no more of great interest. Hence, we are more interested by the static precision. Fig. 20-a shows the experimental response of the TRING-module. The accuracy is about $\pm 5nm$ and the vibrations are due to the high sensitivity of the measurement to the environment. Such performances are of great interest for micromanipulation/microassembly. The Fig. 20-b shows the Black-Nichols diagram of the closed-loop system and indicates the margin phase. According to the figure, the margin gain is $50dB$. These robustness margins are widely sufficient to ensure the stability of the closed-loop system regarding the incertainty of the parameters and of the structure of the developed model. Finally, the interest of the closed-loop control is to ensure these performances when external disturbances will appear during the micromanipulation/microassembly tasks. It may concern the environmental disturbance (temperature variation, etc.) or the manipulation disturbance (manipulation force).

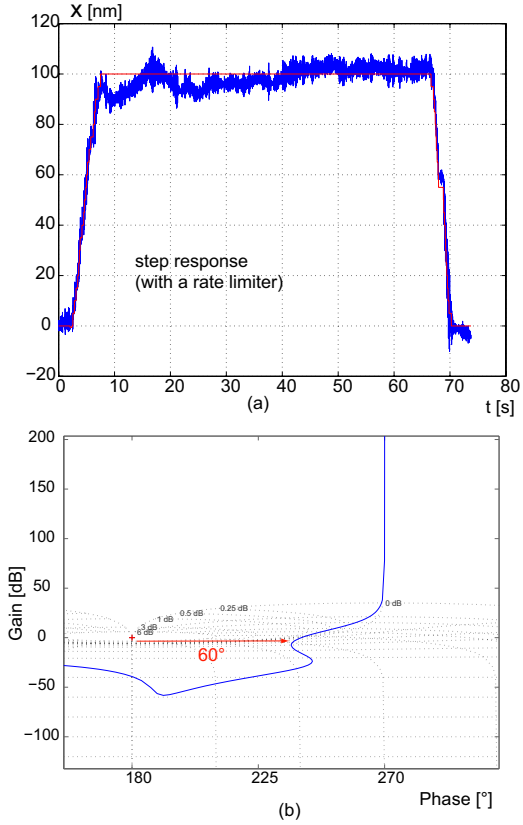

Fig. 20. PI control of the TRING-module in sub-step functioning.

VII. Conclusion

In this paper, we have presented the development, the sub-step modelling and control of a 2DoF (linear angular) micropositioning device, named TRING-module.

The device is based on the stick-slip principle which enables it to have submicrometric resolution and large strokes. The performance analysis show that the TRING-module is well suited for the automated microassembly stations. These performances concern the strokes, the high accuracy and the speeds. Moreover, in order to improve the performances in nanopositioning, we have developped a state-space model of the sub-step of the device working within a step. The model has been experimentally validated. Finally, we have

implemented a PI controller making the sub-step mode have good performances for micromanipulation and microassembly use and a good robustness facing an eventual uncertainty of the parameters of the model.

ACKNOWLEDGMENT

Particular thanks to Dr. Jean-Marc Breguet, from the 'Laboratoire des Systèmes Robotiques' of the Swiss Federal Institute of Technology Lausanne (LSRO-EPFL), for providing us the microatuators, sensors and many precious advises. This project is partially supported by the **EUPASS**-project (**E**volvable **U**ltra-**P**recision **A**ssembly **S**ystem**S** : http://eupass.org/).

REFERENCES

[1] R. S. Fearing, "Survey of sticking effect for micro parts handling" IEEE International Conference on Intelligent Robots and Systems, IROS, Vol.2, pp.212-227, Pittsburgh, PA, USA 1995.

[2] Q. Zhou, Al Aurelian, C. del Corral, P. J. Esteban, P. Kallio, B. Chang and K. N. Koivo, "A microassembly station with controlle environment", SPIE Photonics, 2001.

[3] N. Dechev, L. Ren, W. Liu, W. L. Cleghom, J. K. Mills, "Development of a 6 Degree of Freedom robotic micromanipulator for use in 3D MEMS microassembly", IEEE International Conference on Robotics and Automation, ICRA, pp.281-288, Orlando, Florida, May, 2006.

[4] C. Clévy, A. Hubert, N. Chaillet, "A new micro-tools exchange principle for micromanipulation", IEEE International Conference on Intelligent Robots and Systems, IROS, pp.230-235, Sendai International Center, Japan, 28 september-2 october 2004

[5] J. A. Thompson and R. S. Fearing "Automating microassembly with orthotweezers and force sensing", IEEE International Conference on Intelligent Robots and Systems, IROS, November 2001, Maui, HI.

[6] W. Driesen, T. Varidel, S. Régnier and J. M. Breguet, "Micro manipulating by adhesion with two collaborating mobile micro robots", Journal of Micromechanics and Microengineering, IOP, 15, 2005.

[7] S. Fatikow, B. Magnussen and U. Rembold, "A piezoelectric mobile robot for handling of microobjects", International Symposium on Microsystems, Intelligent Materials and Robots, Sendai 1995.

[8] A. Kortschack, O. C. Hanbler, C. Rass, S. Fatikow, "Driving principles of Mobile Microrobots for the Micro- and Nanohandling", IEEE International Conference on Intelligent Robots and Systems, IROS, Las Vegas, Nevada, USA, pp.1895-1900, October 27-31, 2003.

[9] A. Bergander, W. Driesen, T. Varidel, M. Meizoso and J. M. Breguet, "Mobile $cm3$-microrobots with tools for nanoscale imaging and micromanipulation" Mechatronics Robotics (MechRob 2004), pp.1041-1047, 13-15 Aachen, Germany, September 2004.

[10] M. Rakotondrabe, Y. Haddab and P. Lutz, "Voltage/frequency proportional control of stick-slip micropositioning systems", to appear in IEEE Transactions on Control Systems Technology.

[11] S. Fatikow, T. Wich, H. Hülsen, T. Sievers and M. Jähnisch, "Microrobot system for automatic nanohandling inside a scanning electron microscope", IEEE/ASME Transactions on Mechatronics, 12(3), pp.244-252, 2007.

[12] S. K. Hung, E. T. Hwu, M. Y. Chen and L. C. Fu, "Dual-stage piezoelectric nano-positioner utilizing a range-extended optical fiber Fabry-Perot interferometer" IEEE/ASME Transactions on Mechatronics, 12(3), pp.291-298, 2007.

[13] S. P. Salisbury, D. F. Waechter, R. B. Mrad, S. E. Prasad, R. G. Blacow and B. Yab, "Closed-loop control of a complementary clamp piezoworm actuator", IEEE/ASME Transactions on Mechatronics, 12(6), pp.590-598, 2007.

[14] Babak Sedghi, "Control design of hybrid systems via dehybridization", PhD thesis, Ecole Polytechnique Fédérale de Lausanne, Switzerland 2003.

[15] A. Bergander, W. Driesen, T. Varidel and J.M. Breguet, "Monolithic piezoelectric push-pull actuators for inertial drives," IEEE International Symposium Micromechatronics and Human Science, pp.309-316, 2003.

[16] W. Driesen, A. Bergander, T. Varidel and J.M. Breguet, "Energy consumption of piezoelectric actuators for inertial drives" IEEE International Symposium on Micromechatronics and Human Science, pp.51-58, 2003.

[17] ANSI/IEEE, "An American National Standard - IEEE Standard on Piezoelectricity", 1987.

[18] B. Armstrong-Hélouvry, P. Dupont and C. Canudas-De-Wit, "A survey of models, analysis tools and compensation methods for the control of machines with friction", Automatica, 30(7), 1994.

[19] P. Dupont, V. Hayward, B. Armstrong and F. Altpeter, "Single state elastoplastic models" IEEE Transactions on Automatic Control, Vol.47, N^o5, May 2002.

[20] M. Rakotondrabe, Y. Haddab and P. Lutz, "Design, devbelopment and experiments of a high stroke-precision 2DoF (linear-angular) microsystem", IEEE International Conference on Robotics and Automation, ICRA, Orlando Florida, May 2006.